ELSEVIER

International Journal of Mass Spectrometry 204 (2001) 255–266

International Journal of Mass Spectrometry

Intrinsic reactivity of metal–hydroxide complexes: O–H bond activation and adduct formation in gas-phase reactions of Cp_2ZrOH^+

David E. Richardson*, G.H. Lisa Lang, Elisa Crestoni, Matthew F. Ryan, John R. Eyler

Center for Catalysis, Department of Chemistry, University of Florida, Gainesville, FL 32611-7200, USA

Received 21 March 2000; accepted 20 June 2000

Abstract

Fourier transform ion cyclotron resonance mass spectrometry was used to study the gas-phase reactions of three zirconium(IV) hydroxide ions, Cp_2ZrOH^+ (Cp = η^5-cyclopentadienyl), Cp_2ZrOD^+, and $Cp_2Zr^{18}OH^+$. Product distributions were determined for reactions with alcohols, amines, ethers, esters, and amides. Reactions with alcohols lead to O–H bond activation with formation of alkoxide complexes Cp_2ZrOR^+ and elimination of water. Equilibrium constants for the reactions were used to determine the relative energetics of Zr–OR bonds, and the affinities of hydroxide and alkoxides toward the zirconium(IV) center in Cp_2Zr^{2+} decrease ($OH^- > MeO^- > EtO^- \approx$ *iso*-$PrO^- \approx$ *sec*-$BuO^- \approx$ *tert*-BuO^-) in the same order as the proton affinities of RO^-. Adducts of the alkoxide complex ion with alcohols are formed at long reaction times. Reaction with acetic acid leads to formation of the carboxylate complex ion $Cp_2ZrO_2CCH_3^+$ and elimination of water. Amines, ethers, esters, and amides all form adducts with Cp_2ZrOH^+, but no other reaction pathways, such as hydrolysis, are observed. The unsolvated zirconium(IV) hydroxide species can coordinate substrates and activate O–H bonds, but it does not efficiently cleave esters and amides despite its reactive, bound hydroxide and coordinative unsaturation. The relationship of these results to solution reactions of metal–hydroxides is discussed. (Int J Mass Spectrom 204 (2001) 255–266) © 2001 Elsevier Science B.V.

Keywords: Metal–hydroxide; Alcohols; Esters; Amides; Zirconocenes; Hydrolysis

1. Introduction

Metal-bound hydroxides are found in a variety of biological catalysts [1,2] that are active in the hydrolysis of carboxylic acid and phosphoric acid derivatives. A number of transition-metal complexes have been investigated in the catalytic cleavage of RNA, DNA, amides, and carboxylic and phosphate esters [3–8]. These small complexes can serve as models for metalloenzymes such as zinc carboxypeptidase and zinc alkaline phosphatase, which cleave peptide bonds and phosphoester bonds, respectively.

In general, the pH dependence of catalysis can be used to show that a hydroxo complex ($L_xM–OH^{n+}$) or its kinetic equivalent is responsible for observed reactivity with electrophilic substrates. Kinetic studies of substitution inert cobalt(III) complexes have led to

* Corresponding author. E-mail: der@chem.ufl.edu.

PII S1387-3806(00)00359-6

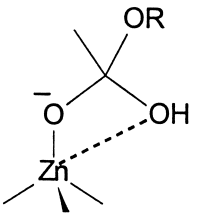

Scheme 1.

detailed mechanisms for their hydrolytic reactions [7], and kinetic studies with labile metal complexes such as zinc(II) chelates indicate similar mechanisms are operative [4]. The generally accepted mechanisms usually involve nucleophilic attack of the metal-bound hydroxide to form a tetrahedral intermediate, which can decompose to products. As in purely organic catalysis, a large number of intermediates can be invoked for the reaction pathways due to the multitude of possible acid–base reactions. The mechanistic complexity is compounded by the presence of a protic solvent such as water. In addition, the metal center may act as a Lewis acid and bind the various intermediates and products by monodentate or bidentate interactions.

In reactions with activated esters (those with good leaving groups), metal hydroxides act as typical O-donor nucleophiles, and the reactivity is generally predictable from the pKa of the metal-bound water [9]. With unactivated substrates (which are better models for biological substrates such as peptide bonds), rates of hydrolysis can be unusually high, and metal binding of substrate and intermediates can be used to rationalize this special reactivity [4]. The concept of bifunctional catalysis can be invoked, in which a nucleophile (hydroxide) and an electrophile (the metal center) are in close proximity and can act in tandem to increase the catalytic reaction rate, e.g. by means of a zinc bound intermediate as shown in Scheme 1. It is this bifunctional catalysis that we are interested in understanding in greater detail via gas-phase studies.

In view of the general interest in metal hydroxide catalysts and the more specific problem of developing gas-phase methods for protein and polynucleic acid cleavage, we have investigated the intrinsic reactivity of a 14-electron zirconium(IV)–hydroxo complex in which the metal center is not coordinatively saturated and is strongly electrophilic (**1**), see Scheme 2.

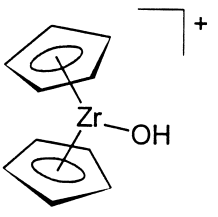

1

Scheme 2.

By studying the reactions of **1** and isotopically labeled analogs with substrates in the absence of solvent, we substantially reduce the complexity of proton inventory in the chemistry. Coordinative unsaturation in **1** can lead to rapid binding of Lewis basic substrates since ligand displacement need not occur. The d^0 zirconium(IV) center serves as a model for bifunctional electrophilic metal complexes based on later transition elements (d^n) and lanthanides (d^0f^n). The reactivity of **1** is a useful model for the intrinsic chemistry of metal hydroxides in the binding and activation of polar substrates.

Reactions of **1** with alcohols are shown here to proceed by O–H activation, most likely by way of a mechanism that can be considered proton transfer or σ-bond metathesis (the latter analogous to C–H activation reactions known for related alkyl complexes in the gas phase and solution). It will also be shown that the simple metal–hydroxide complex **1** is inadequate to cleave esters and amides rapidly in the gas phase, and this absence of observable activity can be explained by barriers associated with likely mechanisms for such hypothetical reactions. The role of solvation in reducing these barriers or opening other pathways will be discussed briefly.

2. Experimental

2.1. Mass spectrometer

All experiments studied in this project were done using a Fourier transform ion cyclotron resonance mass spectrometer (FTICR/MS), which consists of a 3.0 tesla Oxford superconducting magnet (Oxford

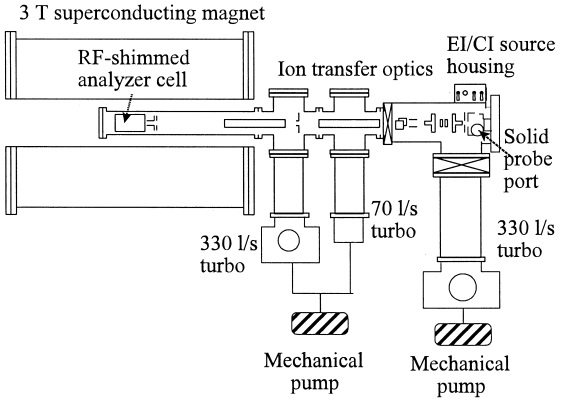

Fig. 1. Schematic of external source FTICR/MS.

Instruments, Cryomagnetic Systems, Abingdon, Oxford, UK), a Bruker Apex external source vacuum chamber (BioAPEX, Bruker Analytical Systems, Inc., Billerica, MA), and a Bruker Aspect 3000 data system. The spectrometer operates in both high resolution and broadband FT modes. A schematic diagram of the instrument is given in Fig. 1. The vacuum system of the instrument is divided into three pumping regions. The source region contains various types of the ionization techniques such as the external electron ionization (EI) and chemical ionization and is evacuated to $\sim 10^{-6}$ mbar with a 330 L/s Edwards turbopump (BOC Edwards Co., Wilmington, MA). The ion-transfer region contains the electrostatic lenses which guide ions into the analyzing chamber and is pumped by a 70 L/s Edwards turbopump. The analyzer region contains the rf-shimmed Infinity cell and is evacuated to a base pressure in the low 10^{-9} mbar by using a 330 L/s Edwards turbopump. The source chamber is connected to the main vacuum with a small orifice that is controlled by a manual gate valve. All sample inlet valves and the solids probe loading ports are pumped by an Edwards mechanical pump.

2.2. Sample handling

The precursor complex $Cp_2Zr(CH_3)_2$ (Cp = η^5 − cyclopentadienyl) is air sensitive, so it was kept in an inert atmosphere box until it was ready to be transferred to the external source ionization chamber. A small quantity of $Cp_2Zr(CH_3)_2$ solid was placed in a melting point capillary, which was sealed with grease before it was taken out of the glove box to prevent moisture contamination. Prior to loading the sample capillary on a solids probe tip, the capillary was cut down to the proper length so it would fit securely in the probe tip. The air exposure time of the sample was kept as short as possible to reduce the amount of decomposition. After the sample tube was secured on the solids probe tip, the probe was inserted into the first region of the probe loading port, which was rapidly evacuated by a mechanical pump to $\sim 3.0 \times 10^{-2}$ mbar. The valve separating the solids probe port from the source chamber was then opened to allow the probe to be inserted into the source chamber, so the sample would be near the filament assembly of the external EI source.

The temperature of the solids probe was maintained around 40–60 °C to ensure sufficient sample vapor in the source region and to provide the maximum signals for the ions of interest. The ions were produced with an appropriate EI energy to maximize the signals of the parent ions $Cp_2ZrCH_3^+$ and to minimize the formation of the fragment ion Cp_2Zr^+; a typical value was ∼30 eV. H_2O, D_2O, and the organic reagents were introduced into the high vacuum region through two Varian precision leak valves, and the amount of vapor leaked into the vacuum was adjusted to provide maximum signals for the ions of interest. Formation of Cp_2ZrOH^+ by reaction of water with $Cp_2ZrCH_3^+$ in the ion trap proved to be more reliable than production in the EI source.

2.3. Equilibrium studies

By introducing two alcohols or an alcohol and water to the ion trap, equilibrium reactions can be observed if the equilibrium constant is not too large or too small. The equilibrium constants (K_{eq}) of alcohol exchange reactions were determined by using the expression

$$K_{eq} = \frac{I_{[Cp_2ZrOR']^+}}{I_{[Cp_2ZrOR]^+}} \frac{p_{ROH}\alpha_{ROH}}{p_{R'OH}\alpha_{R'OH}} \quad (1)$$

where I is the normalized intensity of the two ions, p is the pressure of a neutral gas, and α is the pressure correction factor for the neutrals in the cell based on polarizability. Absolute errors in pressure measurement are expected to have a small impact on the accuracy of equilibrium constant determination due to the chemical and physical similarity of the alcohols and the cancellation of errors in Eq (1).

3. Results and discussion

3.1. Preparation of Cp_2ZrOH^+

Precursor $Cp_2ZrCH_3^+$ ions were produced in the external source region by using electron ionization of $Cp_2Zr(CH_3)_2$ and were then transferred into the analyzer cell. Reaction with water in the high vacuum region produces Cp_2ZrOH^+ by means of the reaction in Eq. 2.

$$Cp_2ZrCH_3^+ + H_2O \rightarrow Cp_2ZrOH^+ + CH_4 \qquad (2)$$

By using appropriately labeled water, $Cp_2Zr^{18}OH^+$ and Cp_2ZrOD^+ were produced for isotope label studies. Analogous reactions occur with alcohols to produce Cp_2ZrOR^+ ions.

After Cp_2ZrOH^+ ions were prepared, they were isolated in the trap by ejection of all other ions and were allowed to react with organic reagents that were also introduced into the analyzer cell. A variable reaction delay controlled the amount of reaction that occurred prior to detection.

All seven major isotopes of zirconium were observed in the spectra, with *m/z* 235 and 237 being the most abundant isotopes for $Cp_2ZrCH_3^+$ and Cp_2ZrOH^+, respectively. In the sections to follow, the Cp_2Zr metallocene fragment is assumed to remain intact for all reactions. Collision induced dissociation experiments of Cp_2ZrOH^+ lead to the loss of OH as indicated by the formation of Cp_2Zr^+.

The thermochemistry of Eq. (2) provides some insight into relative Zr–O and Zr–C bond dissociation energies (BDEs). For the reaction to be observed at near collisional rate constant, the reaction must be ergoneutral or exoergic. The relative HO–H and H_3C–H bond energies require that the Zr–O BDE exceed the Zr–C BDE by $\geq$15 kcal mol^{-1}.

Cp_2ZrOH^+ reacts rapidly with the precursor complex $Cp_2Zr(CH_3)_2$ to form binuclear zirconocenes. This side reaction can be a complicating issue when the EI ionization of $Cp_2Zr(CH_3)_2$ and reaction with water are both done in an ion trap. However, in this work external EI on the precursor followed by ion injection into the trap [which has virtually no $Cp_2Zr(CH_3)_2$ present] is used to remove this pathway.

Table 1
Reactions of Cp_2ZrOH^+ with selected alcohols

Alcohol	Product	*m/z*[a]	Neutral lost
CH_3OH	$Cp_2ZrOCH_3^+$	251	H_2O
CH_3CH_2OH	$Cp_2ZrOCH_2CH_3^+$	265	H_2O
C_6H_5OH	$Cp_2ZrOC_6H_5^+$	313	H_2O
i-$(CH_3)_2CHOH$	$Cp_2ZrOCH(CH_3)_2^+$	279	H_2O
C_4H_9OH[b]	$Cp_2ZrOC_4H_9^+$	293	H_2O

[a] Only the main product isotope ion is listed here.
[b] Includes tert-, sec-, and *n*-butyl alcohols.

3.2. Reactions of alcohols with Cp_2ZrOH^+

Results for the reactions with alcohols are given in Table 1. Alkoxide complexes Cp_2ZrOR^+ are formed exclusively by elimination of water for all the alcohol compounds studied

$$Cp_2ZrOH^+ + ROH \rightarrow Cp_2ZrOR^+ + H_2O \qquad (3)$$

At longer reaction times an alcohol adduct is observed

$$Cp_2ZrOR^+ + ROH \rightarrow Cp_2Zr(OR)(ROH)^+ \qquad (4)$$

The adducts are 16-electron complexes and are formally coordinatively unsaturated; however, 18-electron adducts with two bound alcohols are not observed under our conditions.

Mass spectra obtained for the reactions of Cp_2ZrOH^+ with alcohols are exemplified by the reaction with ethanol shown in Fig. 2. Fig. 2(A) is a spectrum of isolated Cp_2ZrOH^+ ions, and Fig. 2(B) shows formation of the gas-phase product $Cp_2ZrOCH_2CH_3^+$ following a 2.5 s reaction delay after isolation of Cp_2ZrOH^+.

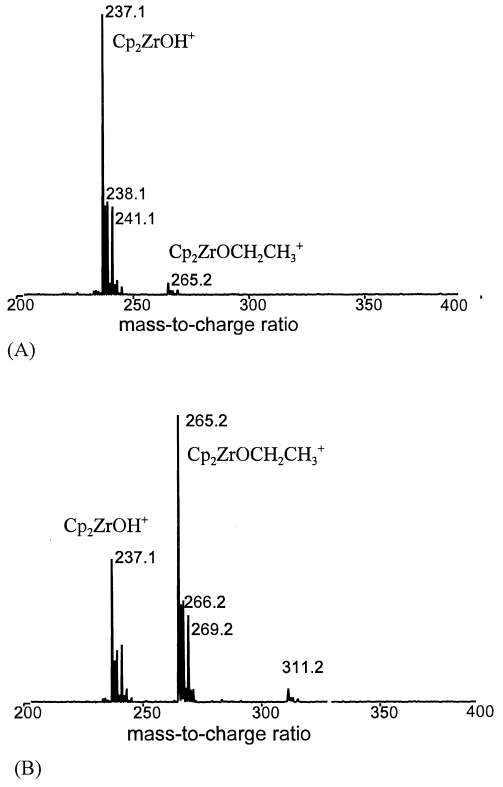

Fig. 2. (A) Spectrum of isolated Cp_2ZrOH^+ ions. A small amount of the product ion at *m/z* 265 has formed following the ejection pulse. (B) Formation of the gas-phase product $Cp_2ZrOCH_2CH_3^+$ following a 2.5 s reaction delay after isolation of Cp_2ZrOH^+. The adduct product ion $Cp_2ZrOCH_2CH_3(C_2H_5OH)^+$ at *m/z* 311 is also observed.

The reaction of Eq. (3) is formally a proton transfer from the alcohol to bound hydroxide. Based on the ready formation of adducts [Eq. (4)] and the coordinatively unsaturated nature of Cp_2ZrOH^+, it is reasonable to suggest that an intramolecular proton transfer occurs following initial formation of an undetected $Cp_2ZrOH(ROH)^+$ adduct. From an alternative but equivalent point of view, the mechanism of the alcohol reaction with Cp_2ZrOH^+ may be considered to proceed by an O–H activation mechanism, which is isoelectronic to the activation of C–H bonds by the complex $Cp_2ZrCH_3^+$ (Scheme 3) [10,11]. This four-center/four-electron σ-bond metathesis mechanism is well documented for d^0 alkyl complexes in general and has been shown to be appropriate in the case of gas-phase reactions of $Cp_2ZrCH_3^+$ with hydrocarbons [10]. In this model, the reaction of Eq. (2) is an example of an O–H activation reaction by $Cp_2ZrCH_3^+$.

Table 2
Reactions of $Cp_2Zr^{18}OH^+$ with selected substrates

Substrate	Product	Neutral lost
CH_3CH_2OH	$Cp_2ZrOC_2H_5^+$	$H_2{}^{18}O$
C_6H_5OH	$Cp_2ZrOC_6H_5^+$	$H_2{}^{18}O$
$CH_3CO_2CH_3$ (methyl acetate)	$\{Cp_2Zr^{18}OH + CH_3CO_2CH_3\}^+$	...
$CH_3CO_2C_2H_5$ (ethyl acetate)	$(Cp_2Zr^{18}OH + CH_3CO_2C_2H_5)^+$	...
CH_3CO_2H (acetic acid)	$Cp_2ZrO_2CCH_3^+$	$H_2{}^{18}O$

Isotopic labeling studies were performed for selected alcohols reacting with $Cp_2Zr^{18}OH^+$ and Cp_2ZrOD^+ to investigate the reaction mechanism in more detail, and some of the results obtained are summarized in Table 2. In all cases the ^{18}O and D labels are lost with water elimination. This result is consistent with a four-center/four-electron transition state for the reaction as illustrated in Fig. 3. In the reaction scheme of Fig. 3, we illustrate the formation of precursor and successor adducts of alcohol and water, respectively. Such adducts are observed at longer reaction times, and the stabilization of the

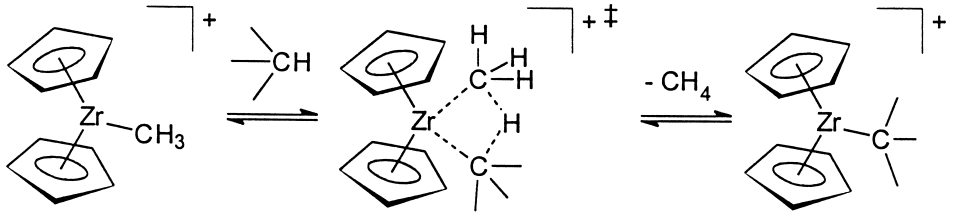

Scheme 3.

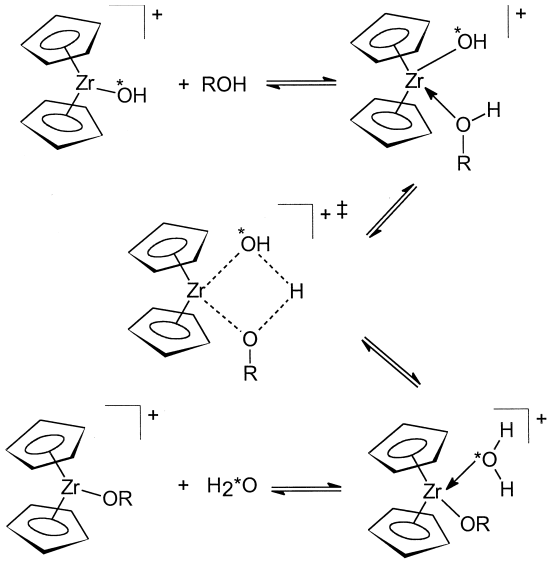

Fig. 3. Proposed mechanism for RO–H activation of alcohols by Cp_2ZrOH^+. The proton transfer from alcohol to bound hydroxide is shown to occur in a four-center/four-electron transition state.

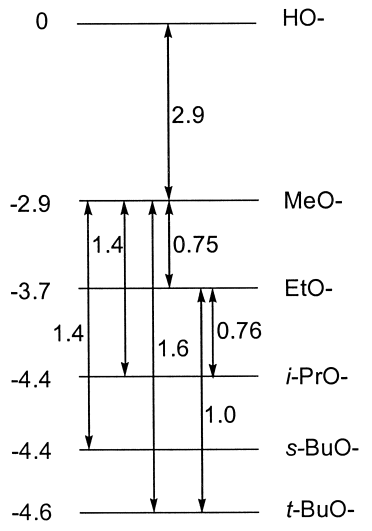

Fig. 4. Equilibrium ladder for reactions [Eq. (5)]. Derived free energy changes from experimental equilibria are shown adjacent to arrows (diagram is not to scale). Estimated free energy changes for Eq. (5) with R = H are shown to the left of the ladder.

adducts arises from either collisional thermalization of the collision complex or radiative cooling of the complex, or both.

3.3. Determination of relative Zr–O bond energies for selected Cp_2ZrOR^+ complexes

Alcohol/water exchange equilibrium reactions can be described by using

$$Cp_2ZrOR^+ + R'OH \rightleftharpoons Cp_2ZrOR'^+ + ROH \qquad \Delta G^{o}_{eq} \tag{5}$$

where R, R′ = H, methyl, ethyl, iso-propyl, sec-butyl, or tert-butyl. Fig. 4 summarizes the ΔG°_{eq} values for the equilibrium reactions studied in this work [determined from $\Delta G^{\circ}_{eq} = -RT\ 1n\ K_{eq}$, with K_{eq} determined by using Eq. (1)]. As seen in Fig. 4, the value of ΔG°_{eq} is negative for the reaction of all alcohols with Cp_2ZrOH^+ [i.e. Eq. (5) with R = H and R′ = Me, Et, iso-Pr, sec-Bu, or tert-Bu). In addition, the ΔG°_{eq} values become increasingly negative as the size of R′ increases.

Typical equilibrium reaction data obtained for the reactions described in Eq. (5) are illustrated by using the reaction of $Cp_2Zr(tert\text{-}OC_4H_9)^+$ with ethanol given in Fig. 5. After ~3 s reaction time, both $Cp_2ZrOC_4H_9^+$ and $Cp_2ZrOC_2H_5^+$ intensities decrease due to the formation of three new adduct products, $Cp_2ZrOC_2H_5(C_4H_9OH)^+$, $Cp_2ZrOC_2H_5(C_2H_5OH)^+$, and $Cp_2ZrOC_4H_9(C_4H_9OH)^+$. However, as the kinetic plot shows in Fig. 5, a reaction equilibrium between the $Cp_2ZrOC_4H_9^+$ complex and the $Cp_2ZrOC_2H_5^+$ complex was established after ~5 s of reaction delay (indicated by a constant intensity ratio or parallel lines on the logarithmic plot). This reaction equilibrium is used to calculate the K_{eq} value of the

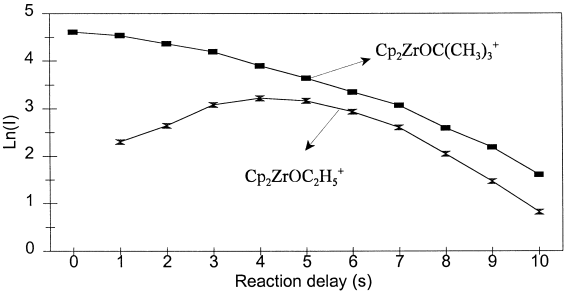

Fig. 5. Reaction of $Cp_2Zr(tert\text{-}OC_4H_9)^+$ with ethanol. Variable reaction delay.

reaction via Eq. (1). It was confirmed that the derived equilibrium constants were independent of relative neutral pressures.

The thermochemistry of Eq. (5) with R = H can be defined by the sum of the three following equations:

$$Cp_2ZrOH^+ \rightleftharpoons Cp_2Zr^+ + \cdot OH \qquad \Delta G^\circ_{hom}\,(Zr\text{–}OH) \tag{6}$$

$$Cp_2Zr^+ + \cdot OR' \rightleftharpoons Cp_2ZrOR'^+ \qquad -\Delta G^\circ_{hom}\,(Zr\text{–}OR') \tag{7}$$

$$\cdot OH + R'OH \rightleftharpoons \cdot OR' + H_2O \qquad \Delta G^\circ_{rad} \tag{8}$$

The value of ΔG°_{eq} is then given by

$$\Delta G^\circ_{eq} = \Delta G^\circ_{hom}\,(Zr\text{–}OH) - \Delta G^\circ_{hom}\,(Zr\text{–}OR') + \Delta G^\circ_{rad} \tag{9}$$

Letting $\Delta G^\circ_{hom}\,(Zr\text{–}OR') - \Delta G^\circ_{hom}\,(Zr\text{–}OH) = \Delta\Delta G^\circ_{hom}$

$$\Delta\Delta G^\circ_{hom} = -\Delta G^\circ_{eq} + \Delta G^\circ_{rad} \tag{10}$$

can be used to calculate the homolytic Zr–OR bond dissociation energies relative to Zr–OH. For calculations using Eq. (10), ΔG°_{rad} is estimated as the value of ΔH°_{rad} by assuming that the contribution of $T\Delta S^\circ_{rad}$ is insignificant under the experimental conditions. ΔH°_{rad} can be calculated from standard enthalpy of formation data. A negative value of $\Delta\Delta G^\circ_{hom}$ means the Zr–OR′ bond is weaker than Zr–OH, and this is the case for all Zr–alkoxides (Table 3). The reactions of Eq. (3) are driven by the formation of the strong HO–H bond.

Although the absolute Zr–O bond energies of Cp_2ZrOR^+ complexes cannot be determined from this study, the relative Zr–O bond energies of Cp_2ZrOR^+ complexes can be estimated. The difference between the Zr–OH and Zr–(O–*t*-Bu) bond energies in this work (13 ± 2 kcal mol^{-1}) is comparable to that obtained for the related neutral $Cp^*_2Zr(X)(OR)$ complexes (Cp* = pentamethylcyclopentadienyl and X is another monodentate ligand) by Schock and Marks (11 kcal mol^{-1}) [12]. Although the absolute bond dissociation energies may be quite different for the neutral complexes compared to the gas-phase ions, the relative energies are essentially unchanged for hydroxide and alkoxide ligands in these zirconium(IV) ionic and neutral organometallics.

The thermochemistry of Eq. (5) with R = H can also be defined by the sum of four equations based on heterolytic bond dissociations:

$$Cp_2ZrOH^+ \rightleftharpoons Cp_2Zr^{2+} + OH^- \qquad \Delta G^\circ_{het}\,(Zr\text{–}OH) \tag{11}$$

$$Cp_2Zr^{2+} + OR'^- \rightleftharpoons Cp_2ZrOR'^+ \qquad -\Delta G^\circ_{het}\,(Zr\text{–}OR') \tag{12}$$

$$OH^- + H^+ \rightleftharpoons H_2O \qquad -\Delta G^\circ_{acid}\,(H_2O) \tag{13}$$

$$R'OH \rightleftharpoons OR'^- + H^+ \qquad \Delta G^\circ_{acid}\,(R'OH) \tag{14}$$

Eqs. (13) and (14) are the gas-phase acid dissociation reactions of water and alcohols. The value of ΔG°_{eq} is then given by

$$\Delta G^\circ_{eq} = \Delta G^\circ_{het}\,(Zr\text{–}OH) - \Delta G^\circ_{het}\,(Zr\text{–}OR') - \Delta G^\circ_{acid}\,(H_2O) + \Delta G^\circ_{acid}\,(R'OH) \tag{15}$$

Letting $\Delta G^\circ_{het}\,(Zr\text{–}OR') - \Delta G^\circ_{het}\,(Zr\text{–}OH) = \Delta\Delta G^\circ_{het}$,

$$\Delta\Delta G^\circ_{het} = -\Delta G^\circ_{eq} - \Delta G^\circ_{acid}\,(H_2O) + \Delta G^\circ_{acid}\,(R'OH) \tag{16}$$

can be used to calculate the relative heterolytic Zr–O bond dissociation energies.

A negative value of $\Delta\Delta G^\circ_{het}$ means the Zr–OR′ bond is weaker than Zr–OH, and values are given in Table 3. The affinities of hydroxide and alkoxides toward the zirconium(IV) center in Cp_2Zr^{2+} therefore decrease ($OH^- > MeO^- > EtO^- \approx$ iso-$PrO^- \approx$ sec-$BuO^- \approx$ tert-BuO^-) in the same order as the proton affinities of RO^-.

3.4. Reaction of Cp_2ZrOH^+ with acetic acid

The reaction of $Cp_2Zr^{18}OH^+$ with acetic acid is illustrated in

$$Cp_2Zr^{18}OH^+ + CH_3COOH \rightarrow Cp_2ZrO_2C_2H_3^+ + H_2{}^{18}O \tag{17}$$

Table 3
Equilibrium data for $Cp_2ZrOH^+ + ROH \rightleftharpoons Cp_2ZrOR+ + H_2O$ and derived Zr–O bond energetics[a]

R	ΔG°_{eq}	$\Delta\Delta G^\circ_{hom}$	$\Delta\Delta G^\circ_{het}$	ΔG°_{acid}[b]	ΔG°_{rad}	D(RO–H)[b]
H	0	0	0	384	0	119.2
Me	−2.9	−12.1	−7	374	−15.0	104.2
Et	−3.7	−11.3	−9	371	−15.0	104.2
i-Pr	−4.4	−(10)	−10	369	(−14)	(105)
s-Bu	−4.4	−(10)	−12	368	(−14)	(105)
t-Bu	−4.6	−12.8	−11	368	−14.1	105.1

[a] All values in kcal mol^{-1}. Estimated error limits are ±1 kcal mol^{-1} on values in first three columns, except values in parentheses are estimates. See text for definitions of free energy changes at the top of the columns.
[b] Values compiled from [16]. Some values are averages from compiled data. Estimated values are in parentheses.

The product ion is most likely a bidentate carboxylate complex. The proposed σ-bond metathesis reaction mechanism of the acetic acid reaction (Fig. 6) is similar to the one proposed above for alcohols. The key step in this mechanism is the migration of hydrogen (formally as a proton) from bound acetic acid to the bound hydroxide.

Observation of a facile reaction indicates the Eq. (17) is exoergic or ergoneutral. The formation of a strong HO–H bond from the weaker AcO–H bond means that the Zr–acetate bond can be weaker than the Zr–OH bond. The homolytic bond dissociation energy of the Zr–acetate bond is no more than ~12 kcal mol^{-1} lower than the Zr–OH value and is likely to be much stronger.

3.5. Reactions of Cp_2ZrOH^+ with other organic substrates

Reactions of Cp_2ZrOH^+ with four other classes of the organic compounds were investigated by using the same method as for the studies of alcohols. Adduct products for Cp_2ZrOH^+ with RCO_2R', ROR', $NRR'R''$, or $RCONR'R''$ were produced exclusively from reactions of Cp_2ZrOH^+ with esters, ethers, amines, or amides, respectively. Substrates investigated included: methyl acetate, ethyl acetate, methyl butyrate, ethyl benzoate, ethyl trifluoroacetate, 4-nitrophenyl acetate, diethyl ether, di-iso-propyl ether, di-*n*-propylamine, triethylamine, N,N-dimethylformamide, N-methylacetamide, and N,N-dimethylacetamide.

Isotopic studies of the reactions of $Cp_2Zr^{18}OH^+$ with selected esters such as methyl acetate and ethyl acetate were done, and the results are summarized in Table 2. For methyl acetate and ethyl acetate, the adducts were observed as the main products without loss of label.

It is noted that initial experiments showed the formation of the acetate complex $Cp_2ZrO_2C_2H_3^+$ when Cp_2ZrOH^+ was allowed to react with a methyl acetate sample, suggesting that hydrolytic cleavage of the ester had occurred with elimination of methanol. However, careful purification of the ester to remove the acetic acid impurity resulted in the disappearance of this product ion, which had been formed via the reaction of Eq. (17).

3.6. Absence of hydrolysis by the L_2Zr–hydroxide cation

Neither esters nor amides are cleaved by an observable reaction with Cp_2ZrOH^+ in the gas phase. Plausible reaction pathways are available for addition–elimination reactions, as described below. Possible origins of kinetic barriers to these reactions will be discussed with a focus on esters.

The Zr–OH unit in Cp_2ZrOH^+ does not undergo facile group exchange reactions with esters to eliminate either acid or alcohol

$$Cp_2ZrOH^+ + MeC(=O)OR \not\rightarrow Cp_2Zr(OR)^+ + MeC(=O)OH \quad (18)$$

$$Cp_2ZrOH^+ + MeC(=O)OR \not\rightarrow Cp_2Zr(O_2CMe)^+ + ROH \quad (19)$$

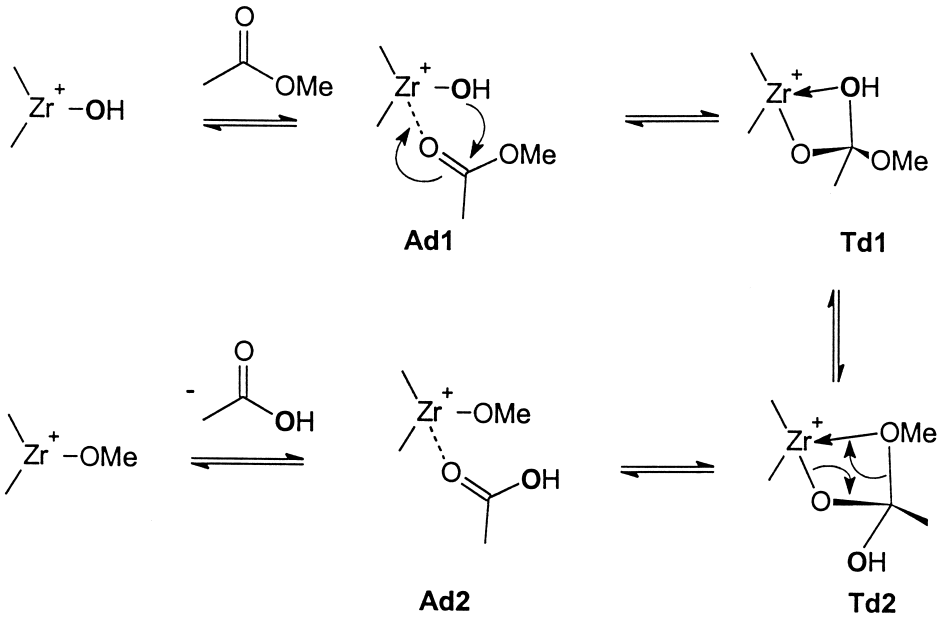

Scheme 4.

(for acetate esters). In the aqueous solution reactivity of metal-hydroxide complexes, either of these reactions can be the basis for catalytic hydrolysis of esters if the resulting metal-alkoxide or metal–carboxylate bonds are labile toward hydrolysis. The absence of the pathways in the gas-phase reaction of Cp_2ZrOH^+ with esters can be understood by consideration of the reaction thermodynamics and likely intermediates in the mechanisms.

The thermochemistry of Eq. (18) is readily estimated from the data in Table 3 and the enthalpy change (5 kcal mol^{-1} for R = methyl) for ester hydrolysis in the gas phase. The hypothetical reaction in Eq. (18) is thereby estimated to be near thermoneutral. A possible mechanism for the transformation is shown in Scheme 4, which is based on solution mechanisms often invoked [4] (ancillary Cp ligands not shown). The reaction could plausibly proceed via formation of the experimentally observed adduct (**Ad1**) followed by intramolecular attack of the bound hydroxide at the electrophilic carbonyl to form a bound tetrahedral intermediate **Td1**.

In the mechanism of Scheme 4, the interconversion of tetrahedral intermediates in the step **Td1** → **Td2** would probably proceed by means of the intermediate **Int1** shown in Scheme 5, in which the coordinated hydroxyl group dissociates. **Int1** could be a true intermediate or a transition state for interconversion of **Td1** and **Td2**.

The formation of the tetrahedral intermediate from OH^- + $CH_3C(O)OMe$ has an exoergicity from ∼−27 to −31 kcal mol^{-1} [13,14]. Therefore, the formation of **Int1** would also be exothermic, with a correction for the difference in bond energies between Cp_2Zr^{2+} and OH^- versus the tetrahedral intermediate alkoxide of **Int1**. Assuming this difference amounts to ∼10 kcal mol^{-1} (estimated from results for other alkoxides in Table 3), the energy of formation of **Int1** from the reactants [Cp_2ZrOH^+ + $CH_3C(O)OMe$] is estimated to be ∼−20 kcal mol^{-1}. However, the

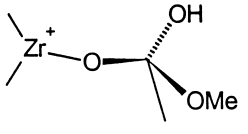

Int1

Scheme 5.

alkoxide of **Int1** is probably a weaker Lewis base than other simple RO^- species such as those in Table 3. Thus, the formation of **Int1** from reactants could be far less exoergic than the estimate given. The transition state for **Int1** formation from **Td1** is expected to be late because a heterolytic bond cleavage is involved. Although probably lower in energy than the reactants, the formation of **Int1** from **Td1** can present a significant kinetic barrier in the gas phase due to tightness of the transition state relative to the dissociation pathway reforming the reactants. The major kinetic barrier to the reaction of Eq. (18) could be the formation of **Int1**, but the conversion from adduct **Ad1** to **Td1** might instead be rate determining.

Turning to Eq. (19), the organic part is essentially displacement of acetate from methyl acetate by hydroxide to form methanol. This type of displacement reaction is well known [15] for gas-phase reactions of OH^- and can proceed by either an S_N2 attack by hydroxide at the α-methyl carbon or via a $B_{ac}2$ pathway, with the latter being somewhat preferred based on a recent theoretical study [14]. Given the apparent strength of the Zr–acetate bond relative to Zr–OH noted earlier, the overall transformation of Eq. (19) is likely to be exoergic.

Direct, linear-transition state S_N2 displacement cannot occur readily because it would lead to significant charge separation and, in the dissociated limit, production of $Cp_2Zr(CH_3OH)^{2+}$ and $CH_3CO_2^-$ (cation–anion separation is electrostatically prohibitive in the gas phase). The electrostatic problem can be resolved if the carboxylate remains bound and methanol is eliminated. Such a mechanism would parallel that for the acetic acid reaction in Fig. 6, except the migrating group would be a methyl group instead of hydrogen. Substantial barriers must be present for this mechanism compared to the O–H activation reactions observed, and this is consistent with the strong preference for migration of hydrogen relative to alkyls in 4-center/4-electron transition states (e.g. Scheme 3) [10].

Formation of **Td1** of Scheme 4 could lead to formation of the carboxylate complex by way of the hydrogen migration transition state, **TS1**, shown in Scheme 6.

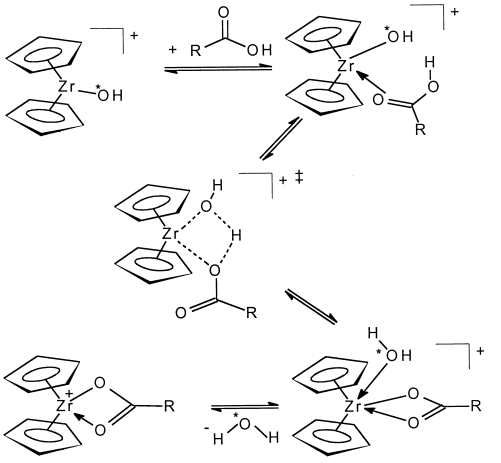

Fig. 6. Proposed mechanism for reaction of Cp_2ZrOH^+ with acetic acid.

This is essentially the $B_{ac}2$ mechanism for acetate displacement with all intermediates bound to zirconium(IV). A significant barrier to this pathway and others must prevent the displacement from occurring at an observable rate in the gas phase.

An analogous analysis can be carried out for amides by replacing OR with NHR, and the mechanism of Scheme 4 can be transformed to that of Scheme 7 for N-methylacetamide. The absence of a facile reaction such as that shown in Scheme 7 presumably results from considerations similar to those for esters, modified by relative preference of zirconium(IV) for oxygen versus nitrogen donors.

A mechanism for the hypothetical reaction of N-methylacetamide to eliminate H_2O and produce the N-methylacetamide complex could involve proton transfer from the substrate to bound hydroxide (analogous to the mechanism in Fig. 6 for acetic acid). The absence of an observable reaction of this type is

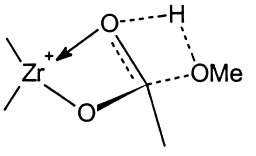

TS1

Scheme 6.

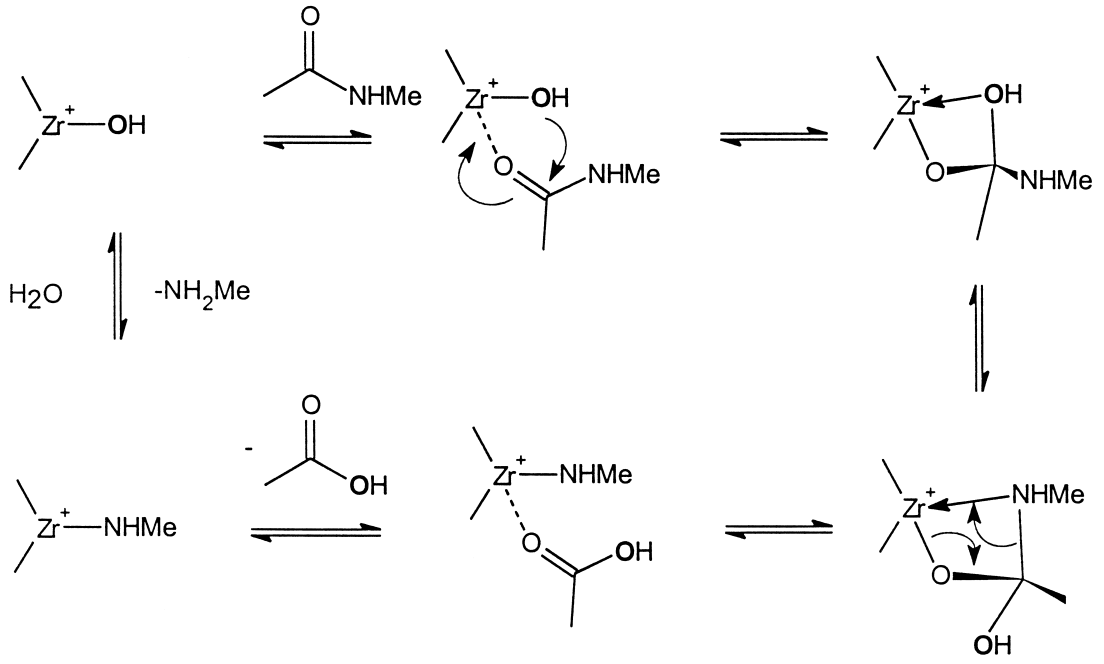

Scheme 7.

consistent with the lower acidity of the amide relative to acetic acid and the oxophilicity of the zirconium(IV) complex.

3.7. Solvation effects on metal–hydroxide reactivity

Despite plausible mechanisms (e.g. Schemes 4 and 7) for ester and amide "hydrolysis" by Cp_2ZrOH^+, such reactions are not observed our gas phase experiments and they must have rate constants approximately three orders of magnitude or more lower than ion-molecule collision rate constants (the approximate limit of the FTICR/MS dynamic range). In some respects, this result is not surprising as second-order rate constants for analogous solution reactions of metal hydroxides tend to be many orders of magnitude below the diffusion-limited rate constant [4].

One obvious difference between gas-phase and solution reactions in protic, polar solvents is the stabilization of charge separation in the latter. Further, protic solvents such as water can serve as proton donors and proton shuttles to accelerate displacement of anionic leaving groups (e.g. alkoxides and amides). Ancillary acidic and basic groups are widely invoked in mechanisms for peptidases and esterases [3].

Lewis basic solvents such as water can also serve to lower barriers to transformations such as **Td1** to **Td2** in Scheme 4. The intermediate **Int1** can be stabilized by coordination of water, and its formation could be accelerated by water.

Acknowledgments

This work was supported by a grant from the National Science Foundation (CHE9727571). The authors thank C. Regino for laboratory assistance with substrate purification.

References

[1] W.N. Lipscomb, N. Strater, Chem. Rev. 96 (1996) 2375.
[2] D.E. Wilcox, Chem. Rev. 96 (1996) 2435.
[3] R. Kramer, Coord. Chem. Rev. 182 (1999) 243.
[4] E.L. Hegg, J.N. Burstyn, Coord. Chem. Rev. 173 (1998) 133.
[5] J.R. Morrow, Metal Ions Biol. Sys. 33 (1997) 561.

[6] E. Kimura, T. Koike, Adv. Inorg. Chem. 44 (1997) 229.
[7] P. Hendry, A.M. Sargeson, Pure Appl. Chem. 38 (1990) 201.
[8] J. Chin, Acc. Chem. Res. 24 (1991) 145.
[9] D. Buckingham, C. Clark, Aust. J. Chem. 35 (1982) 437.
[10] C.S. Christ, J.R. Eyler, D.E. Richardson, J. Am. Chem. Soc. 112 (1990) 596.
[11] D.E. Richardson, N.G. Alameddin, M.F. Ryan, T. Hayes, J.R. Eyler, A.R. Siedle, J. Am. Chem. Soc. 118 (1996) 11244.
[12] L.E. Schock, T.J. Marks, J. Am. Chem. Soc. 110 (1988) 7701.
[13] K. Hori, Y. Hashitani, Y. Kaku, K. Ohkubo, J. Mol. Struct. (Theochem) 461–462 (1999) 589.
[14] F. Haeffner, C.-H. Hu, T. Brinck, T. Norin, J. Mol. Struct. (Theochem) 459 (1999) 85.
[15] O.I. Asubiojo, J.I. Brauman, J. Am. Chem. Soc. 101 (1979) 3715.
[16] NIST Standard Reference Database Number 69 (http://webbook.nist.gov).